

# Scaling Behaviour of the Maximal Growth Rate in the Rosensweig Instability

ADRIAN LANGE

*Universität Magdeburg, Institut für Theoretische Physik, Universitätsplatz 2, D-39106 Magdeburg, Germany*

PACS. 47.20.Ma – Hydrodynamic stability and instability.

PACS. 75.50.Mm – Magnetic liquids.

**Abstract.** – The dependence of the maximal growth rate of the modes of the Rosensweig instability on the properties of the magnetic fluid and the external magnetic induction is studied. An expansion and a fit procedure are applied in the appropriate ranges of the supercritical induction  $\hat{B}$ . With increasing  $\hat{B}$  the scaling of the maximal growth rate changes from linear to a combination of linear and square-root-like scaling. The scaling of the corresponding wave number alternates from quadratic to primarily linear. For very small  $\hat{B}$  the dependence of the maximal growth rate on the viscosity is given. Suggestions are made for experiments to test the predicted scaling behaviours.

*Introduction.* – The investigation of instabilities in magnetic fluids has a long history where the most prominent instability being the normal field or Rosensweig instability [1, 2]. Above a threshold of the induction, the initially flat surface exhibits a stationary array of peaks. Despite its long history, some aspects of the Rosensweig instability have been addressed only recently: the hexagon-square transition [3] or the wave number selection problem [3, 4]. The wave number is the absolute value of the wave vector,  $q = |\mathbf{q}|$ , which characterizes small disturbances. The ground state of a pattern forming system is subjected to such small disturbances in order to study its stability. The corresponding growth rate  $\omega$  may depend on system parameters  $\{\mathcal{P}\}$ , e.g. the viscosity of the fluid, and control parameters  $\{\mathcal{R}\}$ , e.g. an external magnetic field,  $\omega = \omega(q; \{\mathcal{P}\}, \{\mathcal{R}\})$ . Generally it is assumed that in the linear stage of the pattern forming process the wave number with the largest growth rate will prevail. Therefore this mode is called linearly most unstable mode. Due to its role in the pattern formation it is of particular interest to examine the maximal growth rate  $\omega_m$ , and its dependence on the different parameters.

This dependence has received only limited attention in classical hydrodynamic systems. For the Küppers-Lortz (KL) instability in Rayleigh-Bénard convection rotated about a vertical axis, the growth rate of different KL angles were calculated for one fixed rotation rate and different temperature differences [5]. In surface-tension-driven Bénard convection the growth rates are calculated for two fixed values of heat loss and different temperature differences [6]. But in both systems it was not analysed how  $\omega_m$  depends on the control parameters. In the problem of convection for autocatalytic reaction fronts, the maximal growth rate was analysed

only for the two distinct limits of infinite and zero thermal diffusivity [7]. In both cases a power law was found relating the increase of the maximal growth rate with the density difference in the fluid. For the Rayleigh-Taylor instability of superposed incompressible viscous fluids, the maximal growth rate was analysed for appropriately scaled densities and viscosities in [8]. The dependence of  $\omega_m$  on the remaining parameter, the scaled surface tension, is given by a single function covering the whole range of possible values of the surface tension. With respect to experiments, no measurements focusing on the maximal growth rate have yet been undertaken.

Particularly in magnetically or electrically driven systems the fastest growing mode is experimentally accessible. If the field is increased with a sudden jump, a pattern characterized by the linearly most unstable mode should be observed. The validity of this conclusion was shown recently for the Rosensweig instability in magnetic fluids [4]. The lack of studies and the experimental access motivates this letter, where the dependence of the maximal growth rate on the properties of the magnetic fluid and the external magnetic induction is studied.

*System.* – A horizontally unbounded layer of an incompressible, nonconducting, and viscous magnetic fluid of thickness  $h$  and constant density  $\rho$  is considered. The fluid is bounded from below by the bottom of a container made of a magnetically impermeable material and has a free surface with air above. The electrically insulating fluid justifies the stationary form of the Maxwell equations, which reduce to the Laplace equation for the magnetic potentials in the region of the container, the magnetic fluid, and the air. It is assumed that the magnetization of the magnetic fluid depends linearly on the applied magnetic field,  $\mathbf{M} = (\mu_r - 1)\mathbf{H}$ , where  $\mu_r$  is the relative permeability of the fluid.

In a linear stability analysis, all small disturbances from the basic state are decomposed into normal modes, i.e., into components of the form  $\exp[-i(\omega t - \mathbf{q}\mathbf{r})]$  with  $\mathbf{r} = (x, y)$ . If  $\text{Im}(\omega) > 0$ , initially small undulations will grow exponentially and the originally horizontal surface is unstable. Therefore  $\omega$  is commonly called the growth rate, which is in fact true only for its imaginary part in the chosen normal mode ansatz. The linear stability analysis leads to the dispersion relation [9–11]

$$0 = \frac{\nu^2}{\tilde{q} \coth(\tilde{q}h) - q \coth(qh)} \left\{ \tilde{q} [4q^4 + (q^2 + \tilde{q}^2)^2] \coth(\tilde{q}h) - q [4q^2\tilde{q}^2 + (q^2 + \tilde{q}^2)^2] \tanh(qh) - \frac{4q^2\tilde{q}(q^2 + \tilde{q}^2)}{\cosh(qh) \sinh(\tilde{q}h)} \right\} + \tanh(qh) \left[ gq + \frac{\sigma}{\rho} q^3 - \frac{\mu_0\mu_r M^2}{\rho} \Lambda(qh) q^2 \right], \quad (1)$$

where  $\nu$  is the kinematic viscosity,  $\sigma$  the surface tension of the magnetic fluid with air,  $M$  the absolute value of the magnetization,  $\mathbf{g} = (0, 0, -g)$  the acceleration due to gravity,  $\mu_0$  the permeability of free space,  $\tilde{q} = \sqrt{q^2 - i\omega/\nu}$ , and  $\Lambda(qh) = [e^{qh}(1 + \mu_r) + e^{-qh}(1 - \mu_r)]/[e^{qh}(1 + \mu_r)^2 - e^{-qh}(1 - \mu_r)^2]$ . For not too thin layers the approximation with an infinitely thick layer is applicable [3, 4]. Therefore the starting point is the dispersion relation (1) for  $h \rightarrow \infty$  [12]

$$\left(1 - \frac{i\omega}{2\nu q^2}\right)^2 + \frac{1}{4\rho\nu^2 q^4} \left[ \rho g q + \sigma q^3 - \frac{(\mu_r - 1)^2}{(\mu_r + 1)\mu_0\mu_r} B^2 q^2 \right] = \sqrt{1 - \frac{i\omega}{\nu q^2}}. \quad (2)$$

Dimensionless quantities are introduced for all lengths, the induction, the time, and the viscosity,

$$\bar{l} = q_c l, \quad \bar{B} = \frac{B}{B_{c,\infty}}, \quad (3)$$

$$\bar{t} = \frac{g^{3/4} \rho^{1/4}}{\sigma^{1/4}} t = \frac{t}{t_c}, \quad \bar{\nu} = \frac{g^{1/4} \rho^{3/4}}{\sigma^{3/4}} \nu, \quad (4)$$

where  $t_c$  is the so-called capillary time. For  $\bar{\omega} = i\bar{\omega}_2$  with  $\bar{\omega}_2 > 0$ , the real part of eq. (2) reduces to

$$f_+(\bar{q}, \bar{\omega}_2; \bar{\nu}, \bar{B}) := \left( \bar{\nu} + \frac{\bar{\omega}_2}{2\bar{q}^2} \right)^2 + \frac{\bar{q} + \bar{q}^3 - 2\bar{B}^2\bar{q}^2}{4\bar{q}^4} - \bar{\nu}^2 \sqrt{1 + \frac{\bar{\omega}_2}{\bar{\nu}\bar{q}^2}} = 0. \quad (5)$$

The imaginary part of eq. (2) is identically zero. The wave number of maximal growth,  $\bar{q}_m$ , is defined by  $\partial\bar{\omega}_2/\partial\bar{q} = 0$ . Since  $\bar{\omega}_2$  is given implicitly by  $f_+$ , the cross section of  $f_+ = 0$  and  $\partial f_+/\partial\bar{q} = 0$  determines the maximal growth rate and its corresponding wave number.

*Analysis and Results.* – An expansion of  $\bar{B}$ ,  $\bar{q}$ , and  $\bar{\omega}_2$  in the following form

$$\bar{B} = 1 + \hat{B} \quad \bar{q} = 1 + \hat{q}_m \quad \bar{\omega}_2 = 0 + \hat{\omega}_{2,m} \quad (6)$$

leads to an analytical expression of the dependence of  $\hat{\omega}_{2,m}$  and  $\hat{q}_m$  on the induction and the viscosity. All hatted quantities in (6) are small,  $(\hat{B}, \hat{q}_m, \hat{\omega}_{2,m}) \ll 1$ , and denote the scaled distances from the critical values at the onset of the instability. If  $\bar{\nu} \gg \hat{\omega}_{2,m}$ , the expansion of  $f_+ = 0$  and its derivative results in

$$4\bar{\nu}\hat{\omega}_{2,m} - 8\hat{B} + 3\hat{\omega}_{2,m}^2 + 8\bar{\nu}\hat{q}_m\hat{\omega}_{2,m} - 16\hat{q}_m\hat{B} - 4\hat{B}^2 - \frac{\hat{\omega}_{2,m}^3}{2\bar{\nu}} = 0 \quad (7)$$

$$-16\hat{B} - 8\hat{B}^2 + 4\hat{q}_m - 16\hat{B}\hat{q}_m + 8\bar{\nu}\hat{\omega}_{2,m} + 8\bar{\nu}\hat{q}_m\hat{\omega}_{2,m} + \frac{\hat{\omega}_{2,m}^3}{\bar{\nu}} = 0. \quad (8)$$

Considering linear terms in eqs. (7) and (8) only, one obtains  $\hat{\omega}_{2,m} = (2/\bar{\nu})\hat{B}$  and  $\hat{q}_m = 0$ . The latter equation describes an incorrect dependence of the wave number of maximal growth on the applied induction. The result  $\hat{q}_m = 0$  and  $\bar{q} = 1$  (see eq. (6)), respectively, implies that the wave number of maximal growth is constant and equal 1 with increasing induction. Such a conclusion is true only in the case of infinitely viscous magnetic fluids as shown in [4]. Now higher order terms of the applied induction are included by the ansatz

$$\hat{\omega}_{2,m} = \alpha\hat{B} + \beta\hat{B}^2 + \gamma\hat{B}^3 + O(\hat{B}^4), \quad (9)$$

$$\hat{q}_m = \delta\hat{B}^2 + \epsilon\hat{B}^3 + O(\hat{B}^4). \quad (10)$$

Using such an ansatz, the equations (7) and (8) contain all terms that contribute up to third order in  $\hat{B}$ . By determining the expansion coefficients  $\alpha, \dots, \epsilon$ , the dependence on the parameters viscosity and induction is now given by

$$\hat{\omega}_{2,m} = \frac{2}{\bar{\nu}}\hat{B} + \left( \frac{1}{\bar{\nu}} - \frac{3}{\bar{\nu}^3} \right) \hat{B}^2 + \left( \frac{10}{\bar{\nu}^5} - \frac{3}{\bar{\nu}^3} \right) \hat{B}^3 + O(\hat{B}^4) \quad \text{for } 0 \leq \hat{B} < \bar{\nu}^2/6 \quad (11)$$

$$\hat{q}_m = \frac{6}{\bar{\nu}^2}\hat{B}^2 + \left( \frac{6}{\bar{\nu}^2} - \frac{22}{\bar{\nu}^4} \right) \hat{B}^3 + O(\hat{B}^4) \quad \text{for } 0 \leq \hat{B} < \bar{\nu}^2/6. \quad (12)$$

For scaled inductions larger than  $\bar{\nu}^2/6$ , one has to solve the full implicit equation (1) and its derivative with respect to  $q$  numerically. Through the implicit character of both equations, parameter fits are possible only for the dependence of  $\hat{\omega}_{2,m}$  and  $\hat{q}_m$  on  $\hat{B}$ . The fit for an excellent agreement with the numerical data includes a linear term and a square-root term with respect to  $\hat{B}$ , where the coefficients depend on the used magnetic fluid. Combining both

TABLE I – Material [13] and fit parameter of the magnetic fluids.

Fluid	$\rho$ (kg m <sup>-3</sup> )	$\nu$ (m <sup>2</sup> s <sup>-1</sup> )	$\sigma$ (kg s <sup>-2</sup> )	$\bar{\nu}^2/6$	$c_1$	$c_2$	$c_3$	$c_4$
EMG 909	$1.02 \cdot 10^3$	$5.880 \cdot 10^{-6}$	$2.65 \cdot 10^{-2}$	$1.4 \cdot 10^{-4}$	1.03	3.90	3.46	-0.07
EMG 901	$1.53 \cdot 10^3$	$6.540 \cdot 10^{-6}$	$2.27 \cdot 10^{-2}$	$3.9 \cdot 10^{-4}$	1.16	2.95	3.32	-0.10
APG J16	$1.01 \cdot 10^3$	$2.475 \cdot 10^{-5}$	$3.30 \cdot 10^{-2}$	$1.7 \cdot 10^{-3}$	0.72	3.52	3.12	-0.20
APG J14	$1.06 \cdot 10^3$	$2.830 \cdot 10^{-5}$	$3.40 \cdot 10^{-2}$	$2.3 \cdot 10^{-3}$	0.69	3.44	3.08	-0.20
APG S20	$1.05 \cdot 10^3$	$3.333 \cdot 10^{-5}$	$3.30 \cdot 10^{-2}$	$3.3 \cdot 10^{-3}$	0.74	2.91	2.99	-0.22
APG J12	$1.11 \cdot 10^3$	$3.604 \cdot 10^{-5}$	$3.40 \cdot 10^{-2}$	$4.0 \cdot 10^{-3}$	0.58	3.29	2.95	-0.23
APG L17	$1.05 \cdot 10^3$	$5.714 \cdot 10^{-5}$	$3.40 \cdot 10^{-2}$	$9.2 \cdot 10^{-3}$	0.43	3.02	2.71	-0.26
APG J10	$1.16 \cdot 10^3$	$6.034 \cdot 10^{-5}$	$3.40 \cdot 10^{-2}$	$1.2 \cdot 10^{-3}$	0.38	2.92	2.63	-0.27
APG S11n	$1.15 \cdot 10^3$	$6.957 \cdot 10^{-5}$	$3.30 \cdot 10^{-2}$	$1.6 \cdot 10^{-3}$	0.33	2.80	2.51	-0.28
APG 077n	$1.19 \cdot 10^3$	$9.244 \cdot 10^{-5}$	$3.50 \cdot 10^{-2}$	$2.8 \cdot 10^{-3}$	0.26	2.55	2.34	-0.32
APG 037	$0.92 \cdot 10^3$	$1.196 \cdot 10^{-4}$	$3.40 \cdot 10^{-2}$	$3.3 \cdot 10^{-2}$	0.25	2.43	2.24	-0.32

ranges of  $\hat{B}$ , we finally have

$$\hat{\omega}_{2,m} = \begin{cases} \frac{2}{\bar{\nu}}\hat{B} + \left(\frac{1}{\bar{\nu}} - \frac{3}{\bar{\nu}^3}\right)\hat{B}^2 + \left(\frac{10}{\bar{\nu}^5} - \frac{3}{\bar{\nu}^3}\right)\hat{B}^3 & \text{for } 0 \leq \hat{B} < \bar{\nu}^2/6 & (13) \\ c_1\sqrt{\hat{B}} + c_2\hat{B} & \text{for } \bar{\nu}^2/6 \ll \hat{B} \leq 0.4 & (14) \end{cases}$$

$$\hat{q}_m = \begin{cases} \frac{6}{\bar{\nu}^2}\hat{B}^2 + \left(\frac{6}{\bar{\nu}^2} - \frac{22}{\bar{\nu}^4}\right)\hat{B}^3 & \text{for } 0 \leq \hat{B} < \bar{\nu}^2/6 & (15) \\ c_3\hat{B} + c_4\sqrt{\hat{B}} & \text{for } \bar{\nu}^2/6 \ll \hat{B} \leq 0.4, & (16) \end{cases}$$

where the four coefficients  $c_i$ ,  $i = 1, \dots, 4$ , are given in table I for eleven different fluids. These magnetic fluids are made of magnetite nanoparticles dispersed in a carrier liquid (synthetic ester for APG fluids, light petrol for EMG fluids). The nanoparticles are coated with a layer of chemically adsorbed surfactants to avoid agglomeration.

From eqs. (13-16) and the figures 1-3 it is evidently that there are two different scaling regimes for the maximal growth rate as well as for the corresponding wave number. In all three examples, the assumption for the expansion,  $\bar{\nu} \gg \hat{\omega}_{2,m}$ , is well accomplished, see horizontal arrows and solid lines in figs. 1(a)-3(a). A lower bound for the transition between the two regimes is given by  $\bar{\nu}^2/6$ . This value is denoted by the vertical arrows in figs. 1-3.  $\bar{\nu}$  is a combination of the density, the viscosity, and the surface tension of the magnetic fluid, see eq. (4). Therefore the transition range can be matched to experimentally manageable step sizes for the jumplike increase of the magnetic induction by choosing a proper fluid. For the chosen three fluids, the transition range shrinks from a broad interval of  $0.0005 \leq \hat{B}_{trans} \leq 0.004$  for EMG 901 (fig. 1) to  $\hat{B}_{trans} \sim 0.03$  for APG 037 (fig. 3). This shift is mainly caused by an increase in the viscosity (see table I). As a consequence, the range of validity of the two-parameter fit in eqs. (14) and (16) can be replaced by  $\bar{\nu}^2/6 \leq \hat{B} \leq 0.4$  for the fluid APG 037 (see fig. 3). The appearance of different scaling regimes in the Rosensweig instability make it more attractive than instabilities with a single scaling such as the Rayleigh-Taylor instability [8].

The maximal growth rate starts to increase *linearly* with  $\hat{B}$ . Towards the upper bound of the expansion region,  $\hat{B} \lesssim \bar{\nu}^2/6$ , corrections appear due to the quadratic and cubic term in (13). For  $\bar{\nu}^2/6 \ll \hat{B}$ , the dependence of the maximal growth rate on the induction is given by a *linear* as well as by a *square-root* term. Both terms are equally important since approximations with only one term result in inferior fits.

For very small  $\hat{B}$ , the wave number with maximal growth rate increases *quadratically* with  $\hat{B}$ . Near the upper bound of the expansion region cubic corrections occur. For  $\bar{\nu}^2/6 \ll \hat{B}$ ,  $\hat{q}_m$  depends primarily *linearly* on  $\hat{B}$  because  $c_3 \gg |c_4|$ . This linear dependence was already studied in [4] and a good agreement was found between the measured values and the theoretical data.

The fits (14) and (16) give only the dependence of  $\hat{\omega}_{2,m}$  and  $\hat{q}_m$  on the scaled magnetic induction. It would be beneficial to gain insight into the dependence on  $\bar{\nu}$ , too, at least approximately. Therefore the set of eleven fluids and their fit coefficients is used to approximate the relations  $c_i = c_i(\bar{\nu})$ . It is apparent from fig. 4 that all coefficients exhibit a smooth dependence on  $\bar{\nu}$  for  $0.03 \lesssim \bar{\nu} \lesssim 0.45$ . Only for  $\bar{\nu} \simeq 0.04$  and  $\simeq 0.14$ , the values of  $c_1$  and  $c_2$  show deviations. Since  $\hat{\omega}_{2,m} \sim \sigma^{1/4} \omega_{2,m}$ , inaccuracies in the surface tension  $\sigma$  may result in incorrect values of  $c_1$  and  $c_2$ . From experiments with surface wave damping on ordinary fluids it is known that deviations in the value of the surface tension due to contamination may account for differences in the order of 20% [14, 15]. Excluding the large deviations, the following dependencies of  $c_i$  on  $\bar{\nu}$  are suggested (see solid lines in fig. 4)

$$c_1 = 1.11 - 4.13\bar{\nu} + 5.0\bar{\nu}^2 \quad c_2 = 4.0 - 5.0\bar{\nu} + 3.44\bar{\nu}^2, \quad (17)$$

$$c_3 = 3.53 - 4.21\bar{\nu} + 3.06\bar{\nu}^2 \quad c_4 = -0.75 + 0.38/\sqrt[6]{\bar{\nu}}. \quad (18)$$

It is emphasized that the data cover a range of about 2 orders of magnitude in the kinematic viscosity  $\nu$ .

Comparing the numerical data and the analytical results for  $h \rightarrow \infty$  of  $\hat{q}_m$ , one realizes that with increasing fluid viscosity thicker layers are necessary for a good agreement. This is illustrated at a fixed value of  $\hat{B} = 0.0002$  for the three different fluids. For EMG 901 the analytical value according to eq. (15) is already reached at a finite thickness of  $h = 7$  mm. For APG S20 the layer thickness has to be 14 mm before matching with the value of  $\hat{q}_m$  for  $h \rightarrow \infty$ . Finally, for APG 037 a thickness of  $h = 19$  mm is needed to reach  $\hat{q}_m$  in the infinitely thick case. Such a sensitivity does not occur for the maximal growth rate.

*Conclusion.* – The dependence of the maximal growth rate on the properties of the magnetic fluid and the external magnetic induction is studied. An expansion and a fit procedure are applied in the appropriate ranges of the supercritical induction. Both the maximal growth rate  $\hat{\omega}_{2,m}$  and the corresponding wave number  $\hat{q}_m$  follow different scaling regimes. Depending on the material parameters the transition range and its width can be chosen. The scaling of  $\hat{\omega}_{2,m}$  with respect to  $\hat{B}$  changes from linear to a combination of linear and square-root-like with increasing  $\hat{B}$ . The scaling of  $\hat{q}_m$  with respect to  $\hat{B}$  alternates from quadratic to essentially linear with increasing  $\hat{B}$ . For very small  $\hat{B}$ ,  $\hat{\omega}_{2,m}$  depends inversely on the viscosity  $\nu$  of the fluid, whereas  $\hat{q}_m$  varies as  $\nu^{-2}$  with the viscosity, see eqs. (4, 13, 15).

The use of magnetic fluids with properties as APG S20 are suggested to test experimentally the predicted scaling regimes. The range, where the expansion holds lies within the experimentally realizable step size for the jumplike increase of the induction. A clear separation between the different scaling regimes is present (see fig. 2). Thus each regime can be examined independently. Since magnetic fluids are opaque and feature poor reflectivity, a radiosopic detection technique is the best method for this purpose. By utilizing the attenuation of X-rays, the dynamic and static properties of the surface deformation can be measured with high accuracy [16]. Applying this method to the problem presented here would fill the gap of experiments measuring especially maximal growth rates.

\* \* \*

The author thanks B. Reimann and R. Richter for stimulating discussions and is indebted

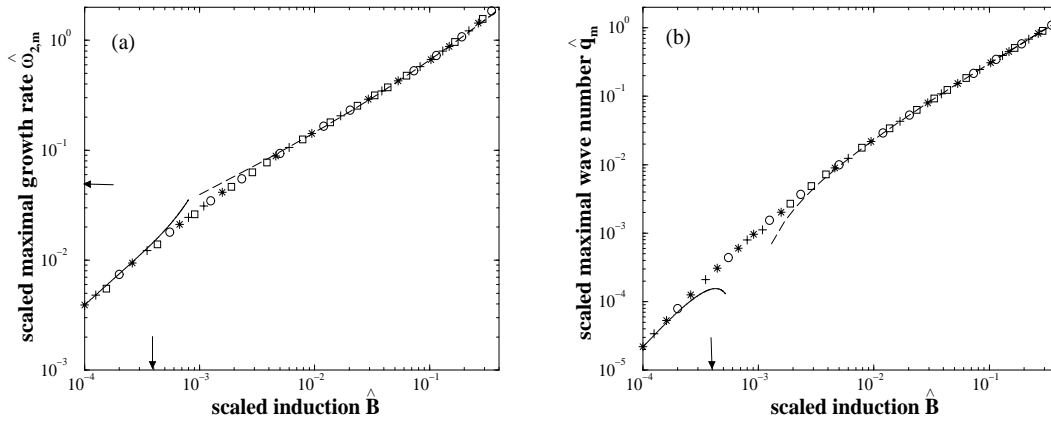


Fig. 1 – Scaled maximal growth rate  $\hat{\omega}_{2,m}$  (a) and scaled maximal wave number  $\hat{q}_m$  (b) as a function of the scaled supercritical induction  $\hat{B}$  for EMG 901. The solid lines denote the analytical results (11) for  $\hat{\omega}_{2,m}$  and (13) for  $\hat{q}_m$  in (a) and (b). The long-dashed lines denote the fits (12) for  $\hat{\omega}_{2,m}$  and (14) for  $\hat{q}_m$  in (a) and (b). Both scaling regimes are clearly separated. The data are calculated for  $h = 100$  mm ( $\circ$ ), 50 mm ( $*$ ), 10 mm ( $+$ ), and 4 mm ( $\square$ ) from eq. (1). The vertical arrows in (a) and (b) indicate  $\bar{\nu}^2/6$ , the horizontal arrow in (a) the dimensionless viscosity  $\bar{\nu}$ .

to B. Huke for bringing into attention calculational errors. R. Richter is acknowledged for sending a preprint of reference [16] and J. Berg for critical reading of the manuscript. This work was supported by the Deutsche Forschungsgemeinschaft under Grant EN 278/2 and LA 1182/2-1.

## REFERENCES

- [1] M. D. Cowley and R. E. Rosensweig, *J. Fluid Mech.* **30**, 671 (1967).
- [2] R. E. Rosensweig, *Ferrohydrodynamics* (Cambridge University Press, Cambridge, 1985).
- [3] B. Abou, J. E. Wesfreid, and S. Roux, *J. Fluid Mech.* **416**, 217 (2000).
- [4] A. Lange, B. Reimann, and R. Richter, *Phys. Rev. E* **61**, 5528 (2000).
- [5] Y. Hu, W. Pesch, G. Ahlers, and R. E. Ecke, *Phys. Rev. E* **58**, 5821 (1998).
- [6] A. Thess and S. A. Orszag, *J. Fluid Mech.* **283**, 201 (1995).
- [7] B. F. Edwards, J. W. Wilder, and K. Showalter, *Phys. Rev. A* **43**, 749 (1991).
- [8] R. Menikoff, R. C. Mjolsness, D. H. Sharp, and C. Zemach, *Phys. Fluids* **20**, 2000 (1977).
- [9] J. Weilepp and H. R. Brand, *J. Phys. II* **6**, 419 (1996).
- [10] B. Abou, G. Néron de Surgy, and J. E. Wesfreid, *J. Phys. II* **7**, 1159 (1997).
- [11] H. W. Müller, *Phys. Rev. E* **58**, 6199 (1998).
- [12] D. Salin, *Europhys. Lett.* **21**, 667 (1993).
- [13] Material data are taken from data sheets of Ferrofluidics Corporation.
- [14] D. M. Henderson and J. W. Miles, *J. Fluid Mech.* **275**, 285 (1994).
- [15] D. R. Howell, B. Buhrow, T. Heath, C. McKenna, W. Hwang, and M. F. Schatz, *Phys. Fluids* **12**, 322 (2000).
- [16] R. Richter and J. Bläsing, *Rev. Sci. Instrum.* **72**, 1729 (2001).

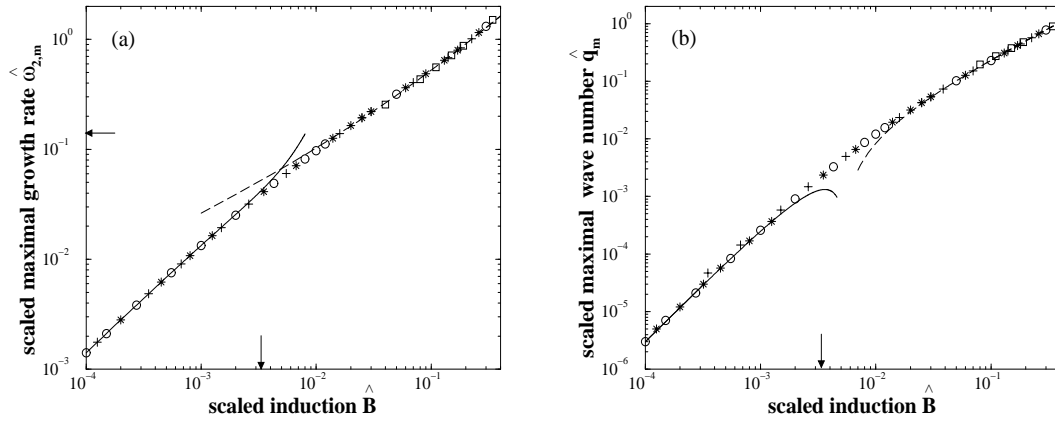


Fig. 2 – Scaled maximal growth rate  $\hat{\omega}_{2,m}$  (a) and scaled maximal wave number  $\hat{q}_m$  (b) as a function of the scaled supercritical induction  $\hat{B}$  for APG S20. The transition range between the different scaling regimes shifts to higher values of  $\hat{B}$  and its width shrinks. The symbols, the arrows and the line types are used as in fig. 1.

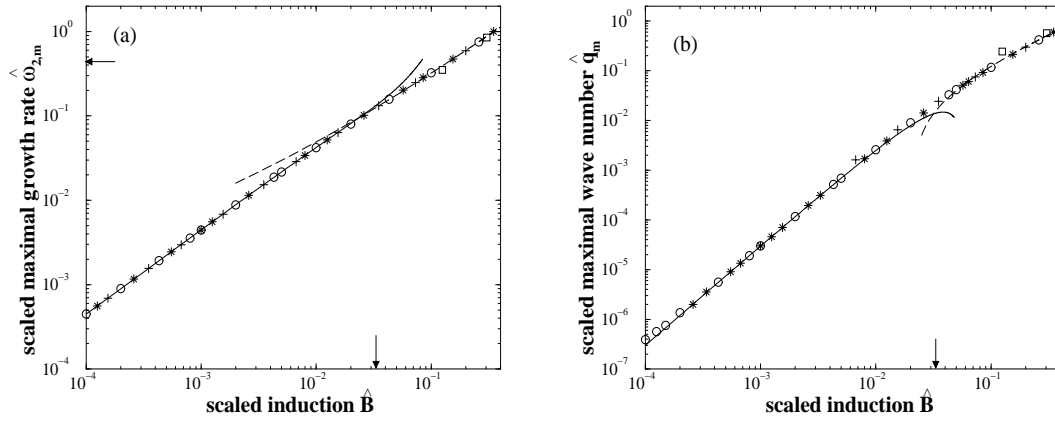


Fig. 3 – Scaled maximal growth rate  $\hat{\omega}_{2,m}$  (a) and scaled maximal wave number  $\hat{q}_m$  (b) as a function of the scaled supercritical induction  $\hat{B}$  for APG 037. The transition range between the different scaling regimes shifts to even higher values of  $\hat{B}$ . Both scaling regimes overlap around  $\hat{B} \sim 0.03$ . The symbols, the arrows and the line types are used as in fig. 1.

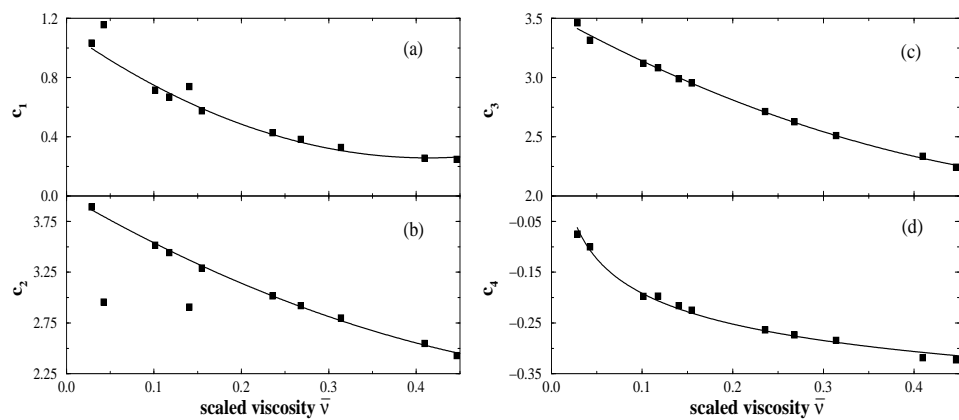


Fig. 4 – Dependence of the coefficients  $c_1$  (a),  $c_2$  (b),  $c_3$  (c), and  $c_4$  (d) on the scaled viscosity  $\bar{\nu}$ . The values of  $c_i$  from table I are plotted as filled squares. The solid lines indicate the approximations by eqs. (17) and (18).